Exp Fluids (2009) 46:963–973
DOI 10.1007/s00348-009-0614-9

RESEARCH ARTICLE

Aerodynamics of intermittent bounds in flying birds

Bret W. Tobalske · Jason W. D. Hearn · Douglas R. Warrick

Received: 6 June 2008 / Revised: 26 November 2008 / Accepted: 10 December 2008 / Published online: 29 January 2009

Abstract Flap-bounding is a common flight style in small birds in which flapping phases alternate with flexed-wing bounds. Body lift is predicted to be essential to making this flight style an aerodynamically attractive flight strategy. To elucidate the contributions of the body and tail to lift and drag during the flexed-wing bound phase, we used particle image velocimetry (PIV) and measured properties of the wake of zebra finch (*Taeniopygia guttata*, $N = 5$), flying at 6–10 m s^{-1} in a variable speed wind tunnel as well as flow around taxidermically prepared specimens ($N = 4$) mounted on a sting instrumented with force transducers. For the specimens, we varied air velocity from 2 to 12 m s^{-1} and body angle from −15° to 50°. The wake of bounding birds and mounted specimens consisted of a pair of counter-rotating vortices shed into the wake from the tail, with induced downwash in the sagittal plane and upwash in parasagittal planes lateral to the bird. This wake structure was present even when the tail was entirely removed. We observed good agreement between force measures derived from PIV and force transducers over the range of body angles typically used by zebra finch during forward flight. Body lift:drag (*L*:*D*) ratios averaged 1.4 in live birds and varied between 1 and 1.5 in specimens at body angles from 10° to 30°. Peak (*L*:*D*) ratio was the same in live birds and specimens (1.5) and was exhibited in specimens at body angles of 15° or 20°, consistent with the lower end of body angles utilized during bounds. Increasing flight velocity in live birds caused a decrease in C_L and C_D from maximum values of 1.19 and 0.95 during flight at 6 m s^{-1} to minimum values of 0.70 and 0.54 during flight at 10 m s^{-1}. Consistent with delta-wing theory as applied to birds with a graduated-tail shape, trimming the tail to 0 and 50% of normal length reduced *L*:*D* ratios and extending tail length to 150% of normal increased *L*:*D* ratio. As downward induced velocity is present in the sagittal plane during upstroke of flapping flight, we hypothesize that body lift is produced during flapping phases. Future efforts to model the mechanics of intermittent flight should take into account that flap-bounding birds may support up to 20% of their weight even with their wings fully flexed.

B. W. Tobalske (✉)
Division of Biological Sciences, Field Research Station at Fort Missoula, University of Montana, Missoula, MT 59812, USA
e-mail: bret.tobalske@mso.umt.edu

J. W. D. Hearn
Harvard Medical School, 25 Shattuck Street, Boston, MA 02115, USA

D. R. Warrick
Department of Zoology, Oregon State University, 2002 Cordley Hall, Corvallis, OR 97331, USA

1 Introduction

Probably the most common style of flight in small birds is a form of intermittent flight that consists of flapping phases interrupted by flexed-wing bounds during which the wings are held motionless and flexed against the body (Rayner 1985; Tobalske 2001). Small birds with rounded, low-aspect ratio wings use intermittent bounds, and small birds with pointed, high-aspect ratio wings use both intermittent bounds and glides in which the wings are extended (Tobalske 2001). The use of intermittent bounds declines with increasing mass among bird species, and the pileated woodpecker (*Dryocopus pileatus*; 0.26 kg) is the largest species for which the flight style has been described (Tobalske 1996, 2001). An adverse scaling of

the mass-specific power available from the flight muscles (or lift per unit power output; Marden 1994) has been hypothesized to account for an upper size limit for this behavior (Rayner 1977, 1985; Tobalske 1996, 2001). Flap-bounding flight may offer a reduction in the mechanical power required for fast forward flight (Rayner 1977; 1985; DeJong 1983; Ward-Smith 1984a, b). However, for flap-bounding to offer an advantage at moderate speeds such as the maximum-range speed considered to be optimal for migration, a dominant model suggests that a bird must support some of its weight during bounds using body lift (Rayner 1985). The aerodynamics of this vertical force are largely unknown.

Working with plaster-cast models of zebra finch (*Taeniopygia guttata*) and an instrumented sting in a wind tunnel, Csicsáky (1977a, b) first demonstrated that a bird in a bound posture can produce body lift (vertical force) of magnitude equal to body drag (horizontal force), with an optimal lift to drag (*L*:*D*) ratio exhibited when the body angle (β) relative to horizontal is approximately 20°. More recently, Tobalske et al. (1999) measured accelerations using kinematics of live birds flying in a wind tunnel and observed that zebra finch generate body lift that supports up to 16% of their body weight and provides *L*:*D* ratios >1 during flight at velocities from 4 to 10 m s^{-1}. These levels of weight support may make flap-bounding an aerodynamically attractive flight strategy at velocities >6 m s^{-1} (Rayner 1985; Tobalske et al. 1999).

Despite considerable effort, there remains uncertainty about the magnitude of body (parasite) drag that birds experience during flight. It is vital to refine the current understanding of body drag, because drag is predicted to affect the magnitude and shape of curves that predict the way power varies with velocity during forward flight. Such curves are necessary for modeling flight behavior, ecology and physiology (Pennycuick 1975; Hedenström and Alerstam 1995; Rayner 1999; Thomas and Hedenström 1998; Tobalske 2007).

Generally, body drag is measured by mounting prepared specimens upon a sting that is instrumented with force transducers. Using such methods, parasite drag coefficients (C_D) of up to 0.5 have been measured (Tucker 1973, 1990; Pennycuick et al. 1988; Maybury 2000; Maybury and Rayner 2001). It is thought that a C_D of this magnitude is likely an overestimate due to the difficulty of preparing specimens to match in vivo feather arrangement and boundary-layer conditions. Streamlined objects prepared to minimize drag should have a $C_D \leq 0.05$ (Hoerner 1965; Pennycuick et al. 1996). One potential constraint to proper feather arrangement in studies using carcasses is that the wings are typically removed with the explicit goal of accounting for parasite drag on the body independently of profile drag on the wings. The lowest C_D yet reported for a carcass is 0.13, and this was measured in European starling (*Sturnus vulgaris*) specimens that were footless and prepared with a coating of paraffin (Maybury 2000).

In contrast, in vivo measures of body C_D during flight are greater than 0.12. Decelerations during bounds in zebra finch suggest a C_D of approximately 0.31 (Tobalske et al. 1999). Rates of steady descent when diving from high altitude during migration give a C_D of 0.37 in other passerine species (Hedenström and Liechti 2001).

Depending upon its shape and how it is spread, the tail may function to provide lift and reduce drag. Delta-wing theory predicts that all surface area cranial to the maximum width of a tail contributes lift and drag, whereas area caudal to the maximum width contributes only drag (Thomas 1993). Some evidence suggests that birds do not always use their tail as predicted according to this theory (Evans et al. 2002). However, other work with tail models indicates that the theory accurately accounts for flow dynamics, at least over a range of tail postures that may commonly be used in flight (Evans 2003). Working with wingless specimens, Maybury (2000) and Maybury et al. (2001) demonstrated that the tail of European starlings sheds a pair of vortices into the wake, consistent with delta-wing theory (Thomas 1993). The tail in starlings also functions as a splitter that helps maintain attached flow via static pressure recovery in the caudal region of the body (Maybury and Rayner 2001).

Because living birds can control their own feather arrangement, intermittent bounds offer a useful model for furthering our understanding of the aerodynamics of body lift and drag in birds. Our first objective in the present study was to test the estimate from Csicsáky (1977a, b) and Tobalske et al. (1999) that zebra finch can generate body lift sufficient for *L*:*D* ratios >1 during intermittent bounds. Our second objective was to test the relative contribution of the body versus the tail to the production of body lift and drag during bounds. To test the relationship between data obtained in vivo versus data obtained from mounted carcasses, we coupled measurements of airflow in the wake of live birds flying in wind tunnel with force-transducer and wake measurements of mounted specimens.

2 Methods

2.1 Animals and wind tunnel

We used five live zebra finch (*T. guttata*, four male, one female, body mass = 17 ± 3 g, length 11.5 ± 0.5 cm, width 3.4 ± 0.2 cm, tail length 3.7 ± 0.3 cm) and four taxidermically prepared specimens (two of each sex, 14 ± 3 g, length 11.0 ± 0.3 cm, width 3.1 ± 0.2 cm, tail length 3.7 ± 0.1 cm). All experiments were performed

using a variable-speed wind tunnel previously described in Tobalske et al. (2005). The live birds flew at 6, 8, and 10 m s^{-1}, their preferred range of flight velocity. The specimens were exposed to velocities from 2 to 12 m s^{-1} at increments of 2 m s^{-1}. This is the full range of forward flight speeds over which zebra finch will fly in our tunnel. We prepared the specimens to be in a bound posture with the tail spread so that the maximum tail span was 75% of the body width (b). The postures and tail spread were informed by film and video images from previous studies (Tobalske et al. 1999; 2005). Given conventional usage of the symbol "b" in the animal-flight literature to represent wing span or half span, it should be noted that when wings are fully flexed during a bound, b also represents wing span.

2.2 Measuring lift and drag

For live birds and specimens, we measured lift (L) and drag (D) using 2D particle image velocimetry (PIV) and also by mounting specimens on a sting instrumented with force transducers. During all experiments with live birds, we verified the location of the bird and the motion of its wings relative to the illumination field using a synchronized high-speed video camera (Redlake PCI-2000) sampling at 250 Hz and located dorsal to the bird. Bounds were identified as intervals with the wings held motionless and fully flexed against the body (Tobalske et al. 1999).

For PIV, we used a LaVision GmBH system with DaVis 7.1 software, a Flowmaster 1,376 × 1,040 pixel digital camera sampling at 5 Hz and a 50-mJ dual-cavity pulsed NdYAG laser. We seeded the air with particles of olive oil (<1 μm in diameter) generated at a rate of 7×10^{10} particles s^{-1} using a vaporizer fitted with a Laskin nozzle. We placed the camera perpendicular to the planar (~3 mm thick) illumination field. For most of our analysis, we used sagittal and parasagittal illumination fields that were 0–3 body lengths caudal to the live birds and specimens. For a subset of the samples of the specimens, we mounted a mirror inside the windtunnel and used it to view a transverse illumination plane 7.5 cm caudal to the shoulder of the specimen (≤0.5 body lengths caudal to the tip of the tail). We accomplished quantitative analysis of 90 PIV samples of bounds from live birds and 3,720 images from specimens. We also performed PIV and visually inspected well over 1,000 images of the wake sampled during flapping phases of flight.

To calculate particle velocity, we used cross-correlation of paired images with an elapsed time between images (Δt) of 250–400 μs to give ~10-pixel particle separation in the regions of greatest velocity. We employed an adaptive multipass with an initial interrogation area of 64 × 64 pixels and final area of 16 × 16 pixels with 50% overlap. Vector fields were post-processed using a median filter (strong removal if difference relative to average >2 * r.m.s. of neighbors and iterative reinsertion if <3 * r.m.s of neighbors), removal of groups with <5 vectors, fill of all empty spaces by interpolation, and one pass of 3 × 3 smoothing. All measures of live birds were from individual (instantaneous) samples. For specimens, we computed an average velocity field from ten images. We estimate minimum error in velocity measurements to be 5.0 ± 0.5% including contributions due to a correlation peak of 0.1 pixels, optical distortion and particle-fluid infidelity (Raffel et al. 2000; Spedding et al. 2003a).

We calculated L using a simplified form of closed-loop integration of velocity about the core of a vortex (Batchelor 1967). We sampled sagittal (±5 mm) illumination planes that bisected a pair of counter-rotating trailing vortices that were always present in the wake of the birds and specimens. Circulation (Γ) was obtained using a line integral of the vertical component of velocity (w) along the Z axis (see Fig. 3a for orientation of axes), with the sample line extended approximately into free-stream flow where $w = 0$ (Spedding et al. 1984; Stamhuis and Nauwelaerts 2005):

$$\Gamma = \int_{-\infty}^{+\infty} w\mathrm{d}Z = \int_{-z(w\approx 0)}^{+z(w\approx 0)} w\mathrm{d}Z. \quad (1)$$

We then estimated L using the Kutta–Joukowski theorem:

$$L = \rho \Gamma u b \quad (2)$$

where ρ = air density, u = horizontal component of velocity, in this case free stream, and b = body width.

Drag was measured using a control-volume with height (h) and width (b) through which we calculated rate change of momentum flow (Batchelor 1967; Vogel 1994):

$$D = b\left(h\rho u_1^2 - \rho \int_0^h u_2^2 \mathrm{d}Z\right). \quad (3)$$

We sampled horizontal velocity in the wake (u_2) along a line on the sagittal plane, and we assumed $u_1 = u_2$ = free-stream u at the upper and lower edges of the control volume. We also assumed static pressure was the same upstream and at our sampling location in the wake. In a subsample of the measurements on specimens, we estimated D by traversing the wake at 5-mm increments from the sagittal plane to the lateral edge on one side of the body (~15 mm). In these instances, Eq. 3 was modified:

$$D = 2\int_0^{b/2}\left(h\rho u_1^2 - \rho\int_0^h u_2^2 \mathrm{d}Z\right)\mathrm{d}Y. \quad (4)$$

Our approach to the control-volume method assumed that there was no sideways (Y-axis) flow in or out of the volume, and we were unable to evaluate this assumption using 2D visualization of flow.

Measures of L and D were obtained for the mounted specimens using a custom-made, calibrated sting that featured an aluminum base instrumented with two dual-element strain gauges per axis (Vishay Measurements Group EA-250PD, 120 Ω) that were in a full-bridge configuration. The resonant frequency of the sting was 15 Hz, and crosstalk between axes was 2%. Signals were conditioned and amplified 2,000× using Vishay Measurements Group 2120B amplifiers, and the voltages from the amplifiers were input to computer using a 16-bit data acquisition system (Digidata 1320A; Axon Instruments). Subsequent low-pass filtering and measurement of the data was performed using Igor (v4) software.

Both L and D were converted to coefficients of lift (C_L) and drag (C_D):

$$C_L = 2L/\rho S u^2 \quad (5)$$

and

$$C_D = 2D/\rho S u^2 \quad (6)$$

where S = frontal projected area of the body. We measured S in live birds as they perched in the wind tunnel with u set at 8 m s^{-1}, the middle of the range of the experiment. We took digital photographs of the birds and imported the images to ImageJ v1.4 software (National Institutes of Health) for calibration to metric coordinates and measurement of S. Similar methods were employed for the mounted specimens, but we measured S at body angles (β) relative to horizontal that varied from −15° to 50° in increments of 5° so that C_L and C_D were calculated using S specific to each β (Fig. 1).

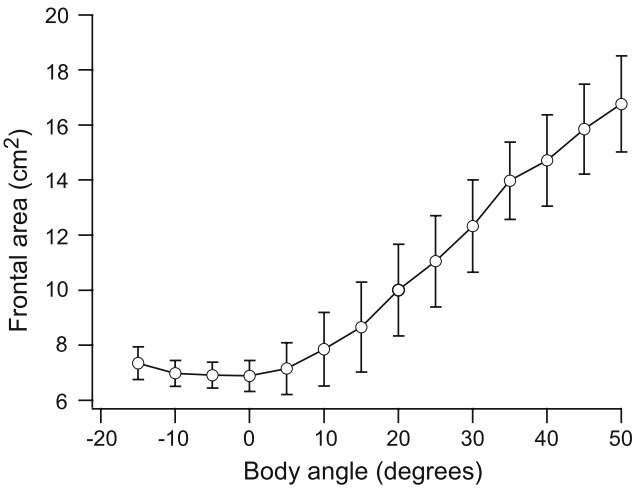

Fig. 1 Effect of body angle (β) upon projected frontal surface area (cm^2) of zebra finch specimens. Projected surface area was used for computing coefficients of lift and drag (C_L and C_D). Shown are mean ± SD (n = 4 specimens)

2.3 Tail manipulation

We altered the tails of mounted specimens to measure the relative contribution of the tail to L and D (Fig. 2). Tails were extended to 150% of initial length by gluing apical extensions obtained from other zebra finch to each of the retrices (Cuervo et al. 2003). We also cut the tail feathers to give a tail length of 50% of normal without apical replacement, and we plucked the feathers (all retrices and tail coverts) to give 0% of normal (Maybury 2000; Maybury and Rayner 2001). We did not vary the tail spread. With the specimens at β = 15°, S was decreased by 9% with no tail, decreased by 4% with the tail length at 50%, and increased by 14% with tail length at 150%. Zebra finch have a graduated tail (Fig. 2), so most of the experimental variation in length caused an increase in tail area cranial to the point of maximum span (Thomas, 1993). For example, comparing 150% to normal (100%) tail length, area cranial to maximum span increased by a factor of 2.2 ± 0.2 while area caudal increased by 1.3 ± 0.2.

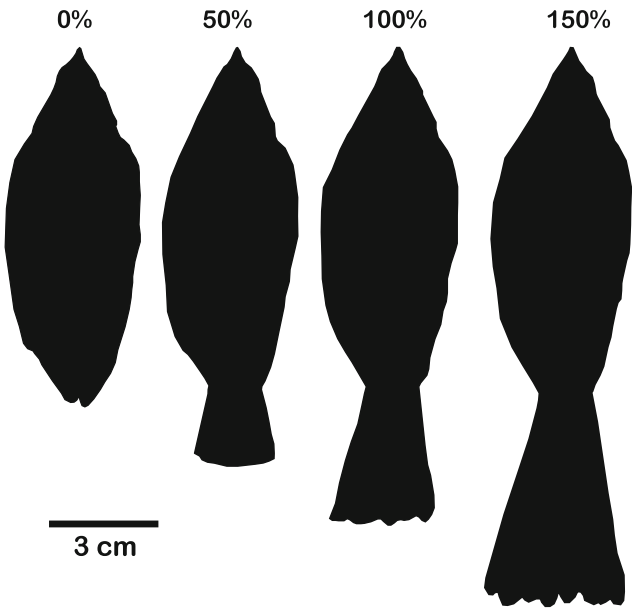

Fig. 2 Body outlines of a zebra finch specimen prepared to be in a bound posture with wings flexed against the body and the tail spread so that its maximum width was 75% of body width. Percentages indicate tail length relative to normal. We glued feathers to specimens to increase tail length and cut feathers to reduce tail length

2.4 Statistical analysis

For each variable, we computed a mean per live bird or specimen and treatment (velocity and/or body angle). We report mean ± SD. Subsequent statistical analyses were performed using StatView v. 5.0.1. To test for differences in the mean values of variables measured in live birds versus the mounted specimens, we used unpaired *t*-tests. We used repeated measures analysis of variance to test for the effects of velocity upon C_L, C_D and L:D ratio in live birds and the effects of tail length on these variables in mounted specimens.

3 Results

3.1 Wake geometry

The wake of live birds during bounds and mounted specimens consisted of a continuously shed pair of counter-rotating vortices with filaments oriented approximately parallel with free-stream flow but convected downward with distance due to downward induced velocity in the middle of the wake (Fig. 3). Parasagittal traverses of the wake at 5-mm intervals showed that the bird's body induced downwash in the middle of the vortex pair out to 10 mm from the midline and upwash on the lateral side of the body and tail at 15 and 20 mm from the midline (Fig. 3a, b). These patterns indicated that the vortex cores were separated by a distance of between 60 and 100% of *b*. Instances of a bounding bird moving along the *Y*-axis through the interrogation plane provided confirmation that the wake consisted of downwash medially and upwash laterally (Fig. 3c).

Profiles of vertical (*w*) and horizontal (*u*) velocity sampled on the sagittal plane of the wake were consistent with predictions for a counter-rotating pair of vortices and a momentum deficit due to drag (Batchelor 1967, Fig. 4). Peak *w* in the center of the wake varied from 2 to 3 m s^{-1} (Fig. 4a), while peak *u* varied from 2 to 4 m s^{-1} less than free-stream *u* (Fig. 4b).

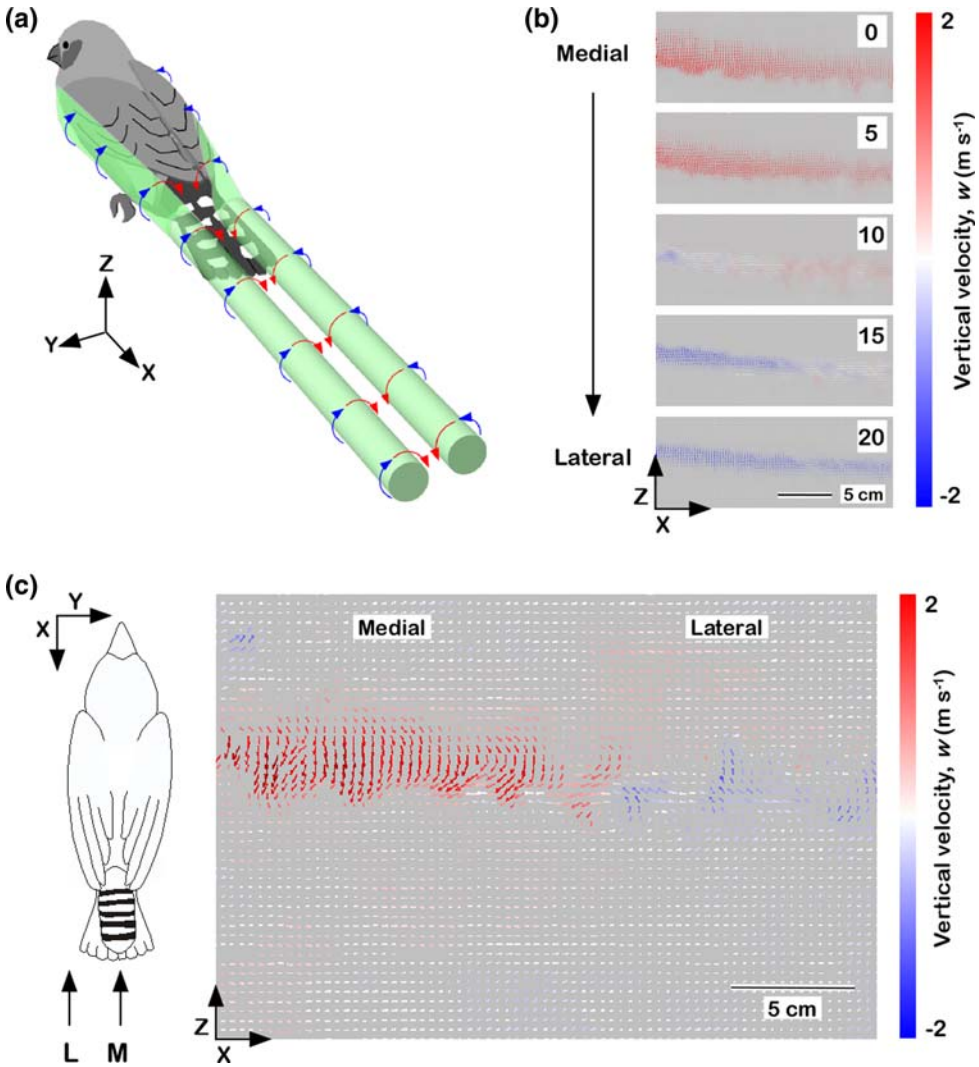

Fig. 3 When in a bound posture, mounted specimens (**a**, **b**) as well as live birds (**c**) shed a pair of counter-rotating vortices into the wake. *Colors* indicate the direction of vertical velocity (*w*) induced by the bird: *red* downwash, *blue* upwash. A cartoon (**a**) indicates the geometry of the flow surrounding the bird and shed into the wake. Three-dimensional axes are provided as orientation for PIV images. Sagittal and parasagittal traverses of the wake (**b**) of a zebra finch specimen mounted with body angle (β) = 15^{O} and horizontal velocity (u) = 8 m s^{-1} (flow from *left* to *right*). A live bird flying at 10 m s^{-1} (**c**) moved through the interrogation plane so that the lateral portion of its wake was sampled first (*blue* upwash at *right*) and then the *middle* of its wake was sampled (*red* downwash at *left*). *Arrows* pointing to the bird outline indicate the location of the lateral (*L*) and medial (*M*) planes sampled in the PIV image. Bird outline from Tobalske et al. (1999)

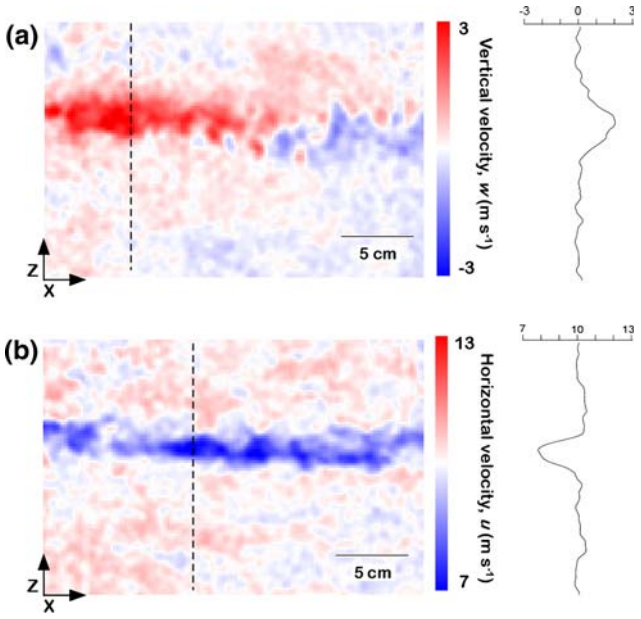

Fig. 4 Profiles of (**a**) vertical velocity (w) and (**b**) horizontal velocity (u) in the wake of a zebra finch engaged in a bound during flight at 10 m s^{-1}. The velocity panels are from the sagittal plane and correspond to the bound shown in Fig. 3c. The *dashed lines* on panels indicate the location from which the profiles were sampled, and the resulting profiles are at *right*. We integrated velocity along these profile lines to estimate body lift and drag. In this instance, L:D ratio was 1.15

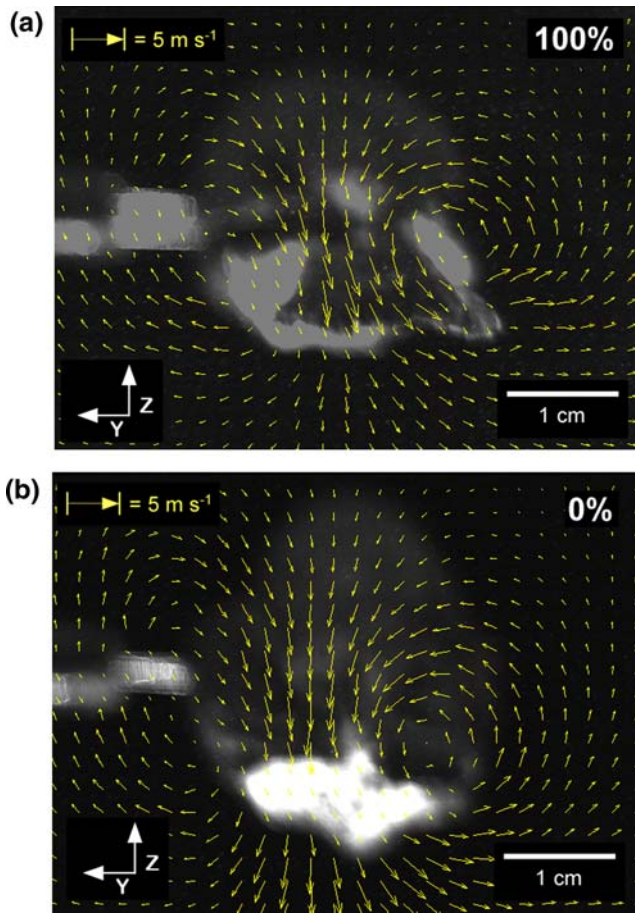

Fig. 5 Caudal views of the pair of vortices shed from a zebra finch specimen mounted with body angle (β) = 15° and horizontal velocity (u) = 8 m s^{-1}. Vectors indicate velocity. The specimen and transducer sting are visible in the background. In a specimen with an intact tail (**a** 100% normal tail length), the vortices in the wake were located dorsal to the tail. The same wake structure was apparent when the tail was removed (**b** 0% of normal tail length), but the presence of the sting consistently distorted the wake so that the midpoint between the counter-rotating vortices was offset laterally from the saggital plane of the body

Transverse views of the wake of specimens mounted at $\beta = 15°$ further clarified that two symmetrical, counter-rotating vortices were shed into the wake (Fig. 5). In birds with intact tails, these vortices were positioned symmetrically about the sagittal plane, dorsal to the tail and with cores spaced approximately = b (Fig. 5a). With removal of the tail length (0%), a counter-rotating pair of vortices was still observed, but drag on the sting caused a distortion of the wake on the side of the sting (Fig. 5b). Traverses providing lateral views of the wake as well as the transverse view in Fig. 5b revealed that the tail was not necessary to the production of induced downwash and the pair of shed vortices. In three specimens (75%) that lacked a tail, drag on the sting pulled the wake along the Y-axis so that, by the time they were fully developed several centimeters into the wake, the counter-rotating pair of vortices were symmetrical about the point of sting attachment rather than the sagittal plane of the bird. In the bird shown in Fig. 5b, the wake was approximately symmetrical about the sagittal plane, but the presence of the sting appeared to distort the shape of the vortex core on that side of the body.

Smaller-scale transverse or cross-stream vorticity in the wake was observed in the lateral view of the wake when sampled at the sagittal plane (Fig. 6). Positive-signed vorticity was shed from the ventral surface of the body and negative-signed vorticity was shed from the dorsal surface. Considerable distortion of the organization of this vorticity was apparent within 20 cm (~2 body lengths) into the wake (Fig. 6).

The wake structure produced during bounds was different from that produced during flapping flight (Fig. 7). Samples from mid-wing, parasagittal plane indicated that the flapping wake was dominated by a vortex ring produced during downstroke (Fig. 7a). However, sagittal samples revealed that vortex cores corresponding to starting and stopping vortices were less evident, perhaps distorted by the wake of the bird's body, and that w was induced downward by the bird during both downstroke and upstroke (Fig. 7b).

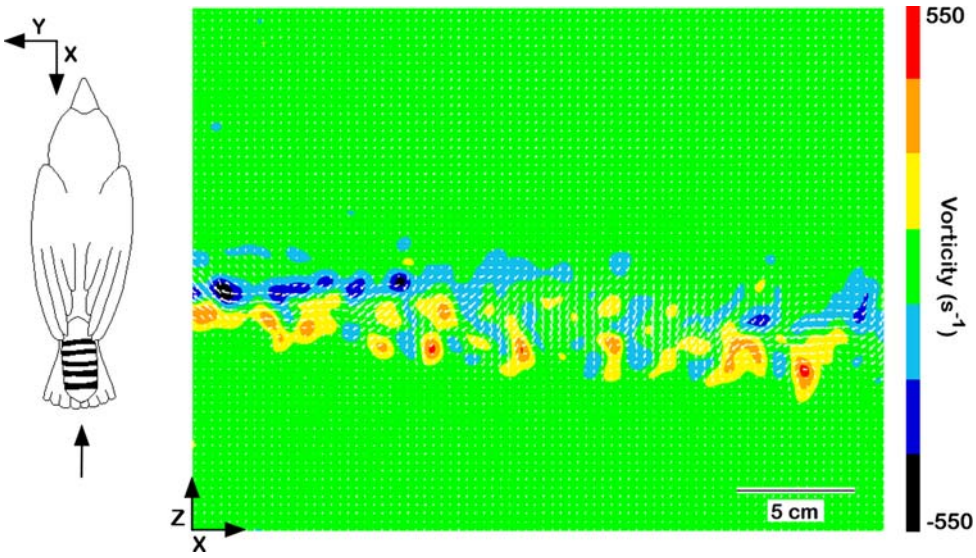

Fig. 6 Velocity and vorticity in the wake of a zebra finch engaged in a bound during flight at 8 m s^{-1}. These data were from a sagittal interrogation plane with *y*-axis location as indicated by the position of the arrow relative to the bird outline (outline from Tobalske et al. 1999). Vectors indicate velocity with free-stream velocity subtracted

3.2 Body lift and drag

Live birds generated *L*:*D* ratios of 1.36 ± 0.03 during bounds while flying at 6–10 m s^{-1} (Fig. 8a). Velocity did not have an effect upon *L*:*D* ratio in live birds (repeated-measures ANOVA, $P = 0.1$, $df = 3, 2$), but there was greater variation in *L*:*D* ratio among birds during flight at 6 m s^{-1} than at the other velocities. The coefficient of variance for *L*:*D* ratio was 38% at 6 m s^{-1} versus 17% at 8 m s^{-1} and 11% at 10 m s^{-1} (Fig. 8a). Lift and drag coefficients (C_L and C_D) varied significantly with flight velocity (repeated-measures ANOVA, $P = 0.0094$ and $P = 0.0021$, respectively, df 3, 2 per test), decreasing with each increase in velocity from 6 to 10 m s^{-1} (Fig. 8b). Specifically, between 6 and 10 m s^{-1}, C_L varied from 1.2 ± 0.4 to 0.7 ± 0.1 and C_D varied from 0.9 ± 0.1 to 0.5 ± 0.1.

Also in live birds, the forces associated with our computed C_L and C_D increased with increasing velocity. Lift varied from 24 ± 8 mN (14.3% of body weight) at 6 m s^{-1} to 39 ± 8 mN (23.5% of body weight) at 10 m s^{-1}. Over the same range of velocity, drag varied from 19 ± 1.9 mN (11.5% of body weight) to 31 ± 4 mN (18.3% of body weight). Over all flight velocities, the percentage of weight supported by body lift during bounds was 20 ± 5%, and body drag was 15 ± 3% of weight.

For mounted specimens, our measures of lift and drag using PIV were in reasonable agreement with our measures using a sting instrumented with force transducers, particularly over the range of β typically used by zebra finch during forward flight (5–30°, Tobalske et al. 1999; Fig. 9). Velocity did not have an effect upon *L*:*D* ratio, but over a range of β from −15° to 50°, *L*:*D* ratio varied from −1 to 1.5 based upon PIV measurements and from −0.8 to 1.2 based upon transducer measurements. *L*:*D* ratios >1 were measured over the range of β from 5° to 25° using PIV and from 10° to 35° using the force sting (Fig. 9a). The polars for C_L as a function of C_D were similar in shape over the range of β up to 35°, although greater scatter was apparent among the polars generated using PIV due primarily to large variation in C_D among velocities within any given body angle (Fig. 9b). For $\beta \geq 35°$, C_D measured using PIV exceeded C_D measured using the force sting, but the large variation in the PIV measures, and relatively small sample size, rendered statistically insignificant the observed differences between mean measurement values. As an example, at 8 m s^{-1}, with $\beta = 40°$ average C_D was 1.0 ± 0.1 using the transducer sting and 1.2 ± 0.3 using PIV (paired *t*-test, $P = 0.1$).

Comparing results from the specimens versus live birds, peak *L*:*D*, averaged among velocities of 6-10 m s^{-1} in the specimens was 1.5 ± 0.3, which was not different from the peak *L*:*D* of 1.5 ± 0.4 in the live birds (*t*-test, $P = 0.9$, $df = 7$).

3.3 Tail manipulation

Although tail length in the specimens mounted at $\beta = 15°$ did not alter the basic wake structure (see Sect. 3.1, above), it did affect *L*:*D* ratio (Fig. 10) as measured using the force sting. Average *L*:*D* ratio among velocities increased with increasing tail length from 1.13 ± 0.04 with no tail (0%) to 1.40 ± 0.04 with tail length at 150% of normal. The effect upon *L*:*D* ratio was statistically significant. For example, at 8 m s^{-1}, the observed differences among the treatment means were significant at $P = 0.003$ (repeated measures ANOVA, $df = 3, 9$). Both C_L and C_D increased with increasing tail length, but the effects of any tail trimming (0 or 50% tail length) were similar, and the most obvious effect among treatments was a relatively greater increase in

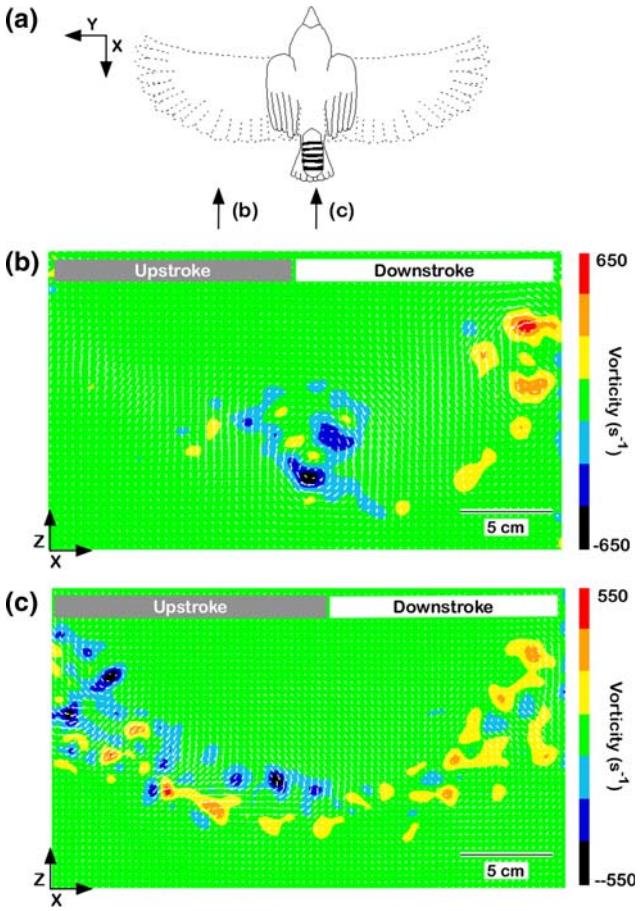

Fig. 7 Velocity and vorticity in the wake of a zebra finch engaged in flapping during flight at 8 m s^{-1}. The bird outline (**a**) shows a dorsal view of wing posture at mid-downstroke (*dashed lines*) and mid-upstroke (*solid lines*), and the arrows indicate the *Y*-axis location of the mid-wing, parasagittal plane (**b**) and saggital plane (**c**). A vortex ring was produced during downstroke, and cross-sectional views of the starting (+) and ending (−) vortices are present in **b**. Although the wings are flexed close to the body during upstroke, downwash is present throughout the wingbeat cycle. We hypothesize that body and tail lift may have contributed to this downwash

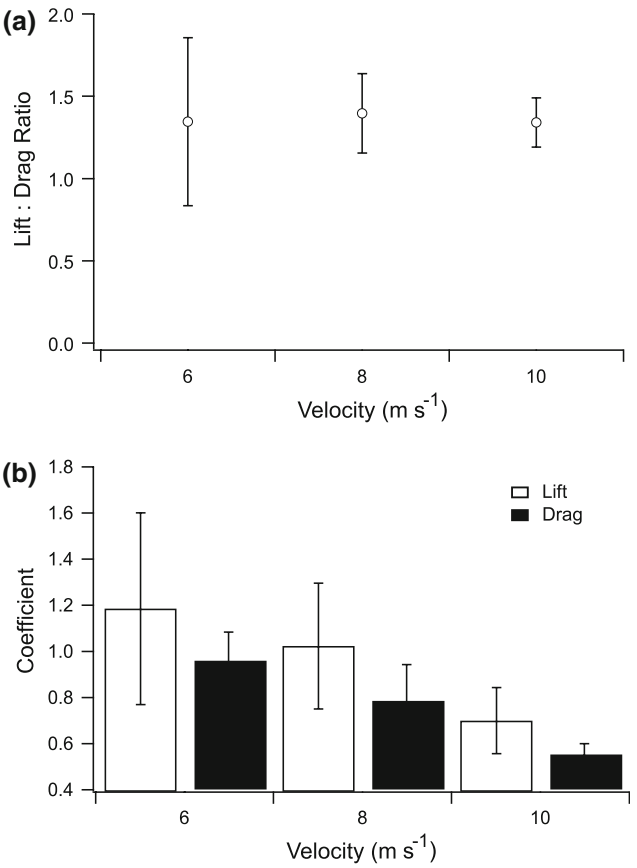

Fig. 8 Lift and drag as estimated from the wake of zebra finch engaged in bounds during flight at 6, 8 and 10 m s^{-1}. **a** Lift:drag (*L*:*D*) ratio. **b** Lift and drag coefficients (C_L and C_D). Shown are mean ± SD, $n = 5$ birds

C_L compared with C_D between 100 and 150% of length. As an example, again at 8 m s^{-1}, intact specimens (100% tail) had a C_L of 0.8 ± 0.1 while C_D was 0.67 ± 0.06. Tail trimming reduced C_L by 38% and C_D by 36% for both the 0% and 50% treatments. Increasing tail length to 150% of normal caused C_L to increase by 42% while C_D increased by only 19%.

4 Discussion

Our measurements showed body lift functions during bounds to support 20% of the bird's body weight (Figs. 3c, 4a, 8). This amount of weight support is slightly higher than the 16% estimate obtained from measures of whole-body acceleration in zebra finch (Tobalske et al. 1999). These levels of body lift are predicted to be sufficient to make flap-bounding an aerodynamically attractive flight strategy compared with continuous flapping at flight speeds greater than 6 m s^{-1} (Rayner 1985; Tobalske et al. 1999). This helps to explain the widespread use of this behavior during flight in small birds up to the size of large woodpeckers (Danielson 1988; Tobalske 1996).

As the zebra finch completely flexes its wings during bounds, it is likely that species that use partial bounds, with wings slightly extended, will achieve comparatively greater levels of weight support during pauses in flapping. Such species include the budgerigar (*Melopsittacus undulatus*; Tobalske and Dial 1994), European starling (Tobalske 1995) and barn swallow (*Hirundo rustica*; Bruderer et al. 2001). Moreover, we predict that downward induced velocity present in the sagittal plane of the wake during upstroke (Fig. 7c) was due in part to body lift during the flapping phases of intermittent flight. Similar wake patterns from flapping phases of flap-bounding flight are evident in the robin (*Erithacus rubecula*; Hedenström et al. 2005). The partially extended wings that are characteristic of mid-

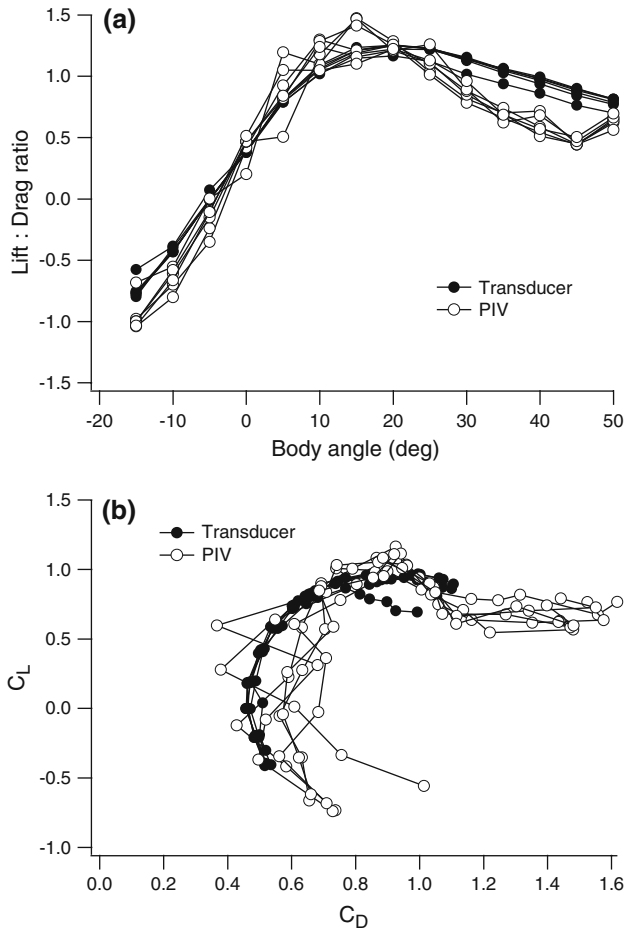

Fig. 9 Lift:drag (L:D) ratio as a function of body angle (β) in zebra finch specimens with traces included for each air velocity from 2 to 12 m s^{-1}. Shown are means ($n = 4$ specimens). *Filled circles* data from sting instrumented with force transducers. *Open circles* data from analysis of the wake using PIV

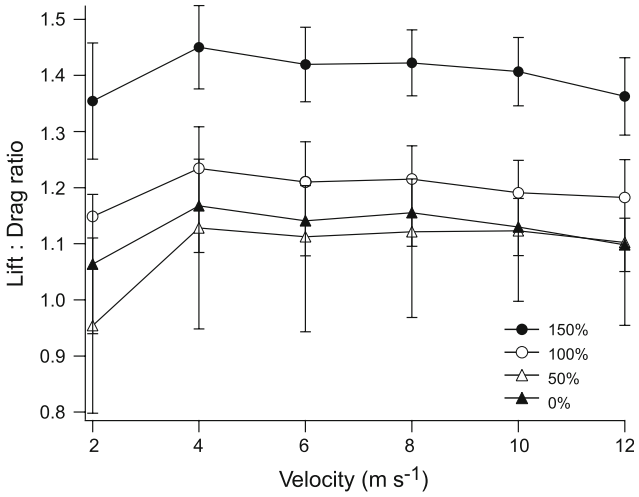

Fig. 10 Effects of tail manipulation on lift:drag (L:D) ratio of zebra finch specimens mounted in a bound posture with body angle (β) = 15°. Percentages indicate tail length relative to normal. Shown are mean ± SD ($n = 4$ specimens)

upstroke in the zebra finch (Fig. 7a) and robin likely also contribute to lift during upstroke. (Tobalske et al. 1999; Spedding et al. 2003b; Hedenström et al. 2005). Testing the relative contribution of the wings versus the body will help refine models of mechanical power output during flap-bounding (Rayner 1985).

Using L:D ratio as a criterion, optimal β during bounds was 15° based on PIV data and 20° based on data from our force sting (Fig. 5). Csicsáky (1977a, b) similarly reports an optimum of 20° for plaster-cast models of zebra finch. The L:D ratio for the plaster cast models in Csicsáky (1977a, b) is 1.18, lower than the average value of 1.4 we measured in live birds (Fig. 8a) and peak values of 1.5 that we measured in mounted specimens (Fig. 9a). Live zebra finch exhibit average β from 20° to 30° (range 12°–37°) during bounds at flight velocities from 6 to 10 m s^{-1} (Tobalske et al. 1999). Thus, zebra finch adopt a body posture during bounds that appears to either maximize body L:D ratio or, at least, keep L:D ratio >1.

Our present experiments are the first efforts applied to bird flight in which force transducers independently confirm that PIV is a reasonably accurate method for measuring in vivo L and D (Figs. 8, 9). However, a force balance against a null hypothesis of weight support in flapping flight is well established using PIV and impulse-based wake analysis (Spedding et al. 2003b; Warrick et al. 2005; Hedenström et al. 2005, 2006). For an animal in steady horizontal flight or hovering, L from flapping wings simultaneously provides both weight support against gravity and thrust to match D, including parasite drag from the body as well as profile drag from the wings. When an animal's mass is known, the vertical component is a known force given gravitational acceleration. Likewise, the net horizontal component of the wake impulse can provide an estimate of the average D due to the body and wings (Hedenström et al. 2005).

The flexed-wing bound posture (Fig. 3) was simple compared with the complex kinematics of the avian wing stroke and rendered adequate a taxidermically prepared model. In contrast, providing transducer-based measures of force during wing flapping may ultimately require the use of dynamically scaled robots (Birch et al. 2004), in vivo implantation of strain gauges (Dial et al. 1997; Biewener et al. 1998; Tobalske et al. 2003) or external mounting of pressure transducers (Usherwood et al. 2005).

Both force sting and PIV measurements confirmed that body lift comes with a substantial cost in the form of body drag (Figs. 4b, 8b, 9). Our measurements of C_D up to 0.9 in live birds is approximately 3 times greater than the average C_D reported for diving passerines (Hedenström and Liechti 2001) and almost 10× the C_D measured in carefully prepared, wingless starling carcasses (Maybury 2000;

Maybury and Rayner 2001). Without doubt, C_D during intermittent bounds was much greater than expected values for streamlined bodies such as airfoils ($\leq$0.05; Hoerner 1965; Pennycuick et al. 1996). It would be worthwhile to test whether body drag during flapping phases is as high as it is during bounds. Using impulse and incline angle of vortices in the wake of flapping phases, Hedenström et al. (2005) report a L:D ratio of 7.5 for the robin. They do not report body and wing area for calculation of C_D, but the weight balance derived for L implies that D represents approximately 13% of body weight during flapping in the robin. This is only slightly less than our measurement of D at 17% of body weight in live zebra finch, but it is important to note that the wing contribution to D must be greater during flapping than during a bound.

An effect of Reynolds number (Re) could potentially account for the unexpectedly high values of C_D we measured in zebra finch. C_L and C_D both decreased as a function of increasing flight speed and, hence, Re (Fig. 8b). For diving passerines, Hedenström and Liechti (2001) observed that C_D decreased from 0.77 to 0.17 as Re increased from 35,000 to 85,000, and the highest Re corresponds to a velocity of 53.7 m s^{-1}. The regression formula for their data is $C_D = 0.82 - 7.5 \times 10^{-6} Re$. Using b as a characteristic length as in Hedenström and Liechti (2001), our measurements at 6, 8 and 10 m s^{-1} in live birds correspond to Re values of 9,900, 13,300 and 16,000. Since the range of Re during experiments in the wind tunnel was less than half the minimum Re measured by Hedenström and Liechti (2001), extreme caution is warranted in extrapolation of their regression equation. Nonetheless, their equation predicts C_D values of 0.75, 0.72 and 0.70 at flight speeds of 6, 8 and 10 m s^{-1}. These predicted values are within 1 standard deviation of our observed C_D at 8 and 10 m s^{-1} (Fig. 8b).

Tail manipulations showed that the tail is not required to produce the pair of counter-rotating trailing vortices associated with body lift (Figs. 3a, 5). With a tail, the vortices appeared to be shed from the edges of the tail and were oriented on the upper surface (Fig. 5). Maybury et al. (2001) observed the same form of vortex production in wingless starling carcasses. Although a counter-rotating pair of vortices shed into the wake by the tail is consistent with predicted function of a tail performing as a delta wing (Thomas 1993), a variety of bluff bodies without tails are known to produce streamwise vortices. Examples include motor vehicles (Hucho and Sovran 1993) and tilted cylinders with an upswept aft section (Zhang et al. 2004). Likewise, specimens with 0% tails at $\beta = 15°$ shed a trailing vortex pair (Fig. 5b) with separation between vortex cores approximately the same as when the tail was present. Since the wingless specimens used by Maybury et al. (2001) and the tailless specimens in our experiments generated the same wake structure, it is apparent that the approximately fusiform shape of a bird's body is sufficient to generate body lift when it is placed at optimal angles relative to horizontal (Figs. 5b, 10).

Lengthening the tail to 150% of normal significantly increased L:D ratio (Fig. 10), so an obvious question emerges: why have not zebra finch and other flap-bounding birds evolved long tails to help maximize their L:D ratio during bounds? There are several alternatives that may constrain tail length in these birds. Given their wing morphology, an increase in tail length may compromise stability or maneuverability (Thomas 1993; Thomas and Taylor 2001; Taylor and Thomas 2002). It may also be subject to relatively higher rates of breakage or wear (Thomas 1993; Barbosa et al. 2003). Additionally, as the birds that use intermittent bounds are relatively small, living at comparatively low Reynolds numbers, it is feasible that tail drag disproportionately limits their ability to fly fast. To the extent that flying fast is necessary, for example to minimize exposure to predators or to migrate in a timely fashion, minimizing tail drag may as important as maximizing lift.

Acknowledgments All procedures involving the animals were approved by the Institutional Animal Care and Use Committee of the University of Portland. This research was supported by National Science Foundation Grants IBN-0327380 and IOB-0615648.

References

Barbosa A, Merino S, Cuervo JJ, De Lope F, Møller AP (2003) Feather damage of long tails in barn swallows. Ardea 91:85–90

Batchelor GK (1967) An introduction to fluid dynamics. Cambridge University Press, Cambridge

Biewener AA, Corning WR, Tobalske BW (1998) In vivo pectoralis muscle force–length behavior during level flight in pigeons (*Columba livia*). J Exp Biol 201:3293–3307

Birch JM, Dickson WB, Dickinson MH (2004) Force production and flow structure of the leading edge vortex on flapping wings at high and low Reynolds numbers. J Exp Biol 207:1063–1072

Bruderer L, Liechti F, Bilo D (2001) Flexibility in flight behaviour of barn swallows (*Hirundo rustica*) and house martins (*Delichon urbica*) tested in a wind tunnel. J Exp Biol 204:1473–1484

Csicsáky M (1977a) Aerodynamische und Ballistische Untersuchungen an Kleinvögeln. PhD thesis, University of Hamburg, Germany

Csicsáky MJ (1977b) Body-gliding in the zebra finch. Fortschr Zool 24:275–286

Cuervo JJ, Møller AP, de Lope F (2003) Experimental manipulation of tail length in female barn swallows (*Hirundo rustica*) affects their future reproductive success. Behav Ecol 14:451–456

Danielson R (1988) Parametre for fritflyvende småfugles flugt. Dan Orn Foren Tidsskr 82:59–60

DeJong MJ (1983) Bounding flight in birds. PhD thesis, University of Wisconsin, Madison, USA

Dial KP, Biewener AA, Tobalske BW, Warrick DR (1997) Mechanical power output of bird flight. Nature 390:67–70

Evans MR (2003) Birds' tails do act like delta wings but delta-wing theory does not always predict the forces they generate. Proc Biol Sci 270:1379–1385

Evans MR, Rosén M, Park K, Hedenström A (2002) How do birds' tails work? Delta-wing theory fails to predict tail shape during flight. Proc Biol Sci 269:1053–1057

Hedenström A, Alerstam T (1995) Optimal flight speed of birds. Philos Trans R Soc Lond B Biol Sci 348:471–487

Hedenström A, Liechti L (2001) Field estimates of body drag coefficient on the basis of dives in passerine birds. J Exp Biol 204:1167–1175

Hedenström A, Rosén M, Spedding GR (2005) Vortex wakes generated by robins *Erithracus rubecula* during free flight in a wind tunnel. J R Soc Interface 3:263–276

Hedenström A, Griethuijsen LV, Rosén M, Spedding GR (2006) Vortex wakes of birds: recent developments using digital particle image velocimetry in a wind tunnel. Anim Biol 56:535–549

Hoerner SF (1965) Fluid-dynamic drag. Hoerner fluid dynamics. Bricktown, New Jersey

Hucho W, Sovran G (1993) Aerodynamics of vehicles. Annu Rev Fluid Mech 25:485–537

Marden JH (1994) From damselflights to pterosaurs: How burst and sustainable flight performance scale with size. Am J Physiol 266:R1077–R1084

Maybury WJ (2000) The aerodynamics of bird bodies. PhD thesis, University of Bristol, UK

Maybury WJ, Rayner JMV (2001) The avian tail reduces body parasite drag by controlling flow separation and vortex shedding. Proc Biol Sci 1474:1405–1410

Maybury WJ, Rayner JMV, Couldrick LB (2001) Lift generation by the avian tail. Proc Biol Sci 268:1443–1448

Pennycuick CJ (1975) Mechanics of flight. In: Farner DS, King JR (eds) Avian biology, vol 5. Academic Press, New York, pp 1–75

Pennycuick CJ, Obrecht HHIII, Fuller MR (1988) Empirical estimates of body drag of large waterfowl and raptors. J Exp Biol 135:253–264

Pennycuick CJ, Klaassen M, Kvist A, Lindström AK (1996) Wingbeat frequency and the body drag anomaly: wind tunnel observations on a thrush nightingale (*Luscinia luscinia*) and a teal (*Anas crecca*). J Exp Biol 199:2757–2765

Raffel M, Willert C, Kompenhans J (2000) Particle image velocimetry: a practical guide. Springer, Berlin

Rayner JMV (1977) The intermittent flight of birds. In: Pedley TJ (ed) Scale effects in animal locomotion. Academic Press, New York, pp 37–55

Rayner JMV (1985) Bounding and undulating flight in birds. J Theor Biol 117:47–77

Rayner JMV (1999) Estimating power curves for flying vertebrates. J Exp Biol 202:3449–3461

Spedding GR, Rayner JMV, Pennycuick CJ (1984) Momentum and energy in the wake of a pigeon (*Columba livia*) in slow flight. J Exp Biol 111:81–102

Spedding GR, Hedenström A, Rosén M (2003a) Quantitative studies of the wakes of freely flying birds in a low-turbulence wind tunnel. Exp Fluids 34:291–303

Spedding GR, Rosén M, Hedenström A (2003b) A family of vortex wakes generated by a thrush nightingale in free flight in a wind tunnel over its entire natural range of flight speeds. J Exp Biol 206:2313–2344

Stamhuis EJ, Nauwelaerts S (2005) Propulsive force calculations in swimming frogs. II. Application of a vortex ring model to PIV data. J Exp Biol 208:1445–1451

Taylor GK, Thomas ALR (2002) Animal flight dynamics. II. Longitudinal stability in flapping flight. J Theor Biol 214:351–370

Thomas ALR (1993) On the aerodynamics of birds' tails. Philos Trans R Soc Lond B Biol Sci 340:361–380

Thomas ALR, Hedenström A (1998) The optimum flight speeds of flying animals. J Avian Biol 29:469–477

Thomas ALR, Taylor GK (2001) Animal flight dynamics. I. Stability in gliding fight. J Theor Biol 212:399–424

Tobalske BW (1995) Neuromuscular control and kinematics of intermittent flight in the European starling (*Sturnus vulgaris*). J Exp Biol 198:1259–1273

Tobalske BW (1996) Scaling of muscle composition, wing morphology, and intermittent flight behavior in woodpeckers. Auk 113:151–177

Tobalske BW (2001) Morphology, velocity, and intermittent flight in birds. Am Zool 41:177–187

Tobalske BW (2007) Biomechanics of bird flight. J Exp Biol 210:3135–3146

Tobalske BW, Dial KP (1994) Neuromuscular control and kinematics of intermittent flight in budgerigars (*Melopsittacus undulatus*). J Exp Biol 187:1–18

Tobalske BW, Peacock WL, Dial KP (1999) Kinematics of flap-bounding flight in the zebra finch over a wide range of speeds. J Exp Biol 202:1725–1739

Tobalske BW, Hedrick TL, Dial KP, Biewener AA (2003) Comparative power curves in bird flight. Nature 421:363–366

Tobalske BW, Puccinelli LA, Sheridan DC (2005) Contractile activity of the pectoralis in the zebra finch according to mode and velocity of flap-bounding flight. J Exp Biol 208:2895–2901

Tucker VA (1973) Bird metabolism during flight: evaluation of a theory. J Exp Biol 58:689–709

Tucker VA (1990) Body drag, feather drag and interference drag of the mounting strut in a peregrine falcon, *Falco peregrinus*. J Exp Biol 149:449–468

Usherwood JR, Hedrick TL, McGowan CP, Biewener AA (2005) Dynamic pressure maps for wings and tails of pigeons in slow, flapping flight, and their energetic implications. J Exp Biol 208:355–369

Vogel S (1994) Life in moving fluids. Princeton University Press, Princeton

Ward-Smith AJ (1984a) Analysis of the aerodynamic performance of birds during bounding flight. Math Biosci 68:137–147

Ward-Smith AJ (1984b) Aerodynamic and energetic considerations relating to undulating and bounding flight in birds. J Theor Biol 111:407–417

Warrick DR, Tobalske BW, Powers DP (2005) Aerodynamics of the hovering hummingbird. Nature 435:1094–1097

Zhang X, Senior A, Ruhrmann A (2004) Vortices behind a bluff body with an upswept aft section in ground effect. Int J Heat Fluid Flow 25:1–9